REPORT DOCUMENTATION PAGE

Form Approved
OMB No. 0704-0188

1. REPORT DATE	2. REPORT TYPE Professional paper	3. DATES COVERED

4. TITLE AND SUBTITLE

Modes in Chiral Core Planar Waveguides: Trainsition from Linear to Circular Polarization

5a. CONTRACT NUMBER

5b. GRANT NUMBER

5c. PROGRAM ELEMENT NUMBER

6. AUTHOR(S)

Dr. Warren Herman

5d. PROJECT NUMBER

5e. TASK NUMBER

5f. WORK UNIT NUMBER

7. PERFORMING ORGANIZATION NAME(S) AND ADDRESS(ES)

Naval Air Warfare Center Aircraft Division
22347 Cedar Point Road, Unit #6
Patuxent River, Maryland 20670-1161

8. PERFORMING ORGANIZATION REPORT NUMBER

9. SPONSORING/MONITORING AGENCY NAME(S) AND ADDRESS(ES)

10. SPONSOR/MONITOR'S ACRONYM(S)

11. SPONSOR/MONITOR'S REPORT NUMBER(S)

12. DISTRIBUTION/AVAILABILITY STATEMENT

Approved for public release; distribution is unlimited.

13. SUPPLEMENTARY NOTES

14. ABSTRACT

The general solution for modes in an asymmetric planar waveguide with an isotropic chiral core is given in terms of a pair of parameters related to the eccentricity of the polarization ellipse for the transverse electric field. This formulation provides insight into the transition, with increasing chirality of the core, from TE/TM modes to right-handed (RHC) and left-handed (LHC) circular polarization modes. The mode properties as a function of waveguide thickness and of frequency are discussed in detail. In addition to the usual cutoff at a minimum thickness (and maximum wavelength), left-handed elliptical modes are found to experience a cutoff at a mode-dependent maximum thickness (and minimum wavelength). The limiting case of a symmetric waveguide is also discussed.

15. SUBJECT TERMS

16. SECURITY CLASSIFICATION OF:			17. LIMITATION OF ABSTRACT	18. NUMBER OF PAGES	19a. NAME OF RESPONSIBLE PERSON Dr. Warren Herman
a. REPORT	b. ABSTRACT	c. THIS PAGE			19b. TELEPHONE NUMBER (include area code)
Unclassified	Unclassified	Unclassified	SAR	11	(301) 342-9114

Standard Form 298 (Rev. 8-98)
Prescribed by ANSI Std. Z39-18

DTIC QUALITY INSPECTED 3

20010109 029

Modes in chiral core planar waveguides: transition from linear to circular polarization

Warren N. Herman

Department of the Navy, EO Sensors Division Code 456,
NAWCAD, Patuxent River, MD 20670

Abstract

The general solution for modes in an asymmetric planar waveguide with an isotropic chiral core is given in terms of a pair of parameters related to the eccentricity of the polarization ellipse for the transverse electric field. This formulation provides insight into the transition, with increasing chirality of the core, from TE/TM modes to right-handed (RHC) and left-handed (LHC) circular polarization modes. The mode properties as a function of waveguide thickness and of frequency are discussed in detail. In addition to the usual cutoff at a minimum thickness (and maximum wavelength), left-handed elliptical modes are found to experience a cutoff at a mode-dependent maximum thickness (and minimum wavelength). The limiting case of a symmetric waveguide is also discussed.

1. INTRODUCTION

The effect of chiral media on electromagnetic waves has been the subject of investigation for two decades, with a good deal of the initial interest centered about radar wavelengths.[1,2,3] In keeping with the interest in that part of the electromagnetic spectrum, early studies of waveguides containing chiral media were on dielectric waveguides with conducting boundaries.[4,5,6,7] At optical wavelengths in bulk material, one of the important physical effects of chirality is optical activity.[8] Chiral polymers[9] are potentially excellent materials for chiral optical waveguides provided sufficient[10] chirality can be realized in a polymer with low optical loss and good film-forming properties. Not surprisingly, chirality, or handedness, of the medium in all-dielectric waveguides has been found to introduce considerable additional mathematical complexity resulting in mode properties that can substantially differ from the achiral dielectric case. Much of the work on planar chiral dielectric waveguides in the literature deals with symmetric boundaries,[11,12,13,14,15] in which the top and bottom claddings have the same dielectric properties. For asymmetric planar waveguides, perturbation techniques have been employed[11,16,17] or approximations have been made[18] to simplify the mathematics.

Here we develop the general solution to the asymmetric planar dielectric waveguide with an isotropic chiral core without making simplifying approximations. The allowed modes are elliptically polarized and, in our formulation, the modal equations contain a pair of parameters that determine the eccentricity of the polarization ellipse for the transverse electric field. The solution for a symmetric waveguide is presented as the limiting case when the top and bottom cladding indices are equal. When the values of the parameters are appropriate for transverse electric (TE) and transverse magnetic (TM) modes in the limit of vanishing chirality, the modal equations are easily seen to reduce to the well-known equations for the TE and TM modes of an achiral waveguide.

2. FIELDS FOR CHIRAL MEDIA

We use $\exp(i\omega t)$ time dependence for Maxwell's equations, which results in the equations involving time derivatives taking the forms

$$\nabla\times E + i\omega B=0 \ , \ \nabla\times H - i\omega D=0 \ , \quad (1)$$

and adopt constitutive equations including chirality in the Drude-Born-Federov form,[19]

$$D = \varepsilon(E+\gamma\,\nabla\times E) \ , \quad B = \mu(H+\gamma\,\nabla\times H) \ , \quad (2)$$

where ε and μ are the usual permittivity and permeability and γ is the chirality parameter, which has units of length. The wave equation for E resulting from Eqs.(1) and (2) contains a $\nabla\times E$ term. Wave equations in chiral media that reduce[12,18] to the Helmholtz equation can be obtained by employing Bohren's decomposition[20] of E and H, which may be taken to have the form[18]

$$E = \frac{1}{2}(F^+ + F^-) \ , \qquad H = \frac{1}{2i}\sqrt{\frac{\varepsilon}{\mu}}(F^+ - F^-) \ , \quad (3)$$

with

$$F^\pm \equiv E \pm i\sqrt{\mu/\varepsilon}\,H \ . \quad (4)$$

From Eqs.(1) and (2) it follows that the vector field functions $F^\pm$ satisfy

$$\nabla\times F^\pm = \mp k_0 n_\pm F^\pm \ , \quad (5)$$

where

$$n_\pm = \frac{n_g}{1\pm\delta} \ , \ n_g = \sqrt{\frac{\varepsilon}{\varepsilon_0}} \ , \ \delta = k_0 n_g \gamma \ , \ \text{and} \ k_0 = \frac{2\pi}{\lambda} \ . \quad (6)$$

All example calculations in the figures in this paper are done for a wavelength of 633 nm. Note that, in terms of these quantities, the rotatory power in bulk material is $\rho \approx k_0 n_g \delta$ for $\delta \ll 1$. The vector fields F^+ and F^- separately obey the Helmholtz equation,

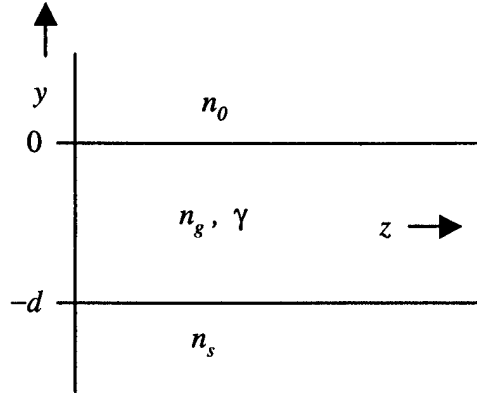$$\nabla^2 F^\pm + (k_0 n_\pm)^2 F^\pm = 0 \ . \quad (7)$$

Figure 1. Coordinate system for an asymmetric planar waveguide with an isotropic chiral core.

In a bulk medium, $\mathbf{F}^+$ and $\mathbf{F}^-$ are plane waves with right-handed circular (RHC) and left-handed circular (LHC) polarization, respectively.

3. THE ASYMMETRIC PLANAR WAVEGUIDE

The structure of the planar waveguide under consideration is shown in Fig. 1. The top and bottom claddings are not chiral and have refractive indices n_0 and n_s, respectively, while the core is isotropic and has permittivity $\varepsilon = \varepsilon_0 n_g^2$ and chirality γ. The bottom cladding will frequently be referred to as the substrate. The waveguide has thickness d and is assumed to be infinite in the $\pm x$ direction. The notation here mostly follows that of Ref. 18 with a notable exception that here we use the symbol γ for the chirality parameter instead of ρ used there in order to clearly distinguish between the chirality parameter in the constitutive equations from the usual symbol ρ for rotatory power.

Waveguide modes propagating in the $+z$ direction have the form

$$\mathbf{F}^\pm(y,z) = \mathbf{\Psi}^\pm(y)\exp(-ik_0 n_{eff} z) , \qquad (8)$$

where n_{eff} is the effective index of a mode with propagation constant $\beta = k_0 n_{eff}$. It follows[21,18] from Eqs.(5) that the y- and z-components of $\mathbf{\Psi}^\pm$ can be found from the x-component, and consequently $\mathbf{\Psi}^\pm$ can be written

$$\Psi_x^\pm(y) \equiv \psi^\pm(y),$$

$$\Psi_y^\pm(y) = \pm i \frac{n_{eff}}{n_q}\psi^\pm(y), \qquad , \qquad (9)$$

$$\Psi_z^\pm(y) = \pm\frac{1}{k_0 n_q}\frac{d\psi^\pm(y)}{dy}$$

where $\psi^\pm(y)$ satisfy the Helmholtz equation, .

$$\frac{d^2\psi^\pm(y)}{dy^2} + k_0^2(n_q^2 - n_{eff}^2)\psi^\pm(y) = 0 . \qquad (10)$$

Here, $q = \pm$ in the core layer, and $q = 0, s$ in the top and bottom claddings, respectively.

The solution to Eqs.(10) can be expressed in the form

$$\psi^\pm(y) = \begin{cases} A^\pm \exp(-vy) , & y \geq 0 \\ B^\pm \cos(u^\pm y + \phi^\pm) , & 0 < y < -d \\ C^\pm \exp(w(y+d)) , & y \leq -d \end{cases} \qquad (11)$$

where

$$u^\pm \equiv k_0\sqrt{n_\pm^2 - n_{eff}^2} , \quad v \equiv k_0\sqrt{n_{eff}^2 - n_0^2} , \quad w \equiv k_0\sqrt{n_{eff}^2 - n_s^2} . \qquad (12)$$

A mode in the chiral core waveguide consists[6] of RHC- and LHC-polarized waves traveling down the guide with the same effective index n_{eff}, but total internal reflection off the interfaces is at different angles of incidence $\theta^\pm$ due to differing refractive indices $n^\pm$, i.e., $\sin\theta^\pm = n_{eff}/n_\pm$ and $\cos\theta^\pm = u^\pm/(k_0 n_\pm)$.

There are four such circularly polarized waves making up a mode in the core: one pair of RHC- and LHC-polarized waves

$$\mathbf{\Phi}_1^\pm = B^\pm \exp(-i\phi^\pm)(\hat{\mathbf{s}} \pm i\hat{\mathbf{p}}_1^\pm)\exp(-i\mathbf{K}_1^\pm \cdot \vec{r}) \qquad (14)$$

traveling toward the top interface with propagation vectors $\mathbf{K}_1^\pm = k_0 n_\pm(0, \cos\theta^\pm, \sin\theta^\pm)$, and another pair

$$\mathbf{\Phi}_2^\pm = B^\pm \exp(i\phi^\pm)(\hat{\mathbf{s}} \pm i\hat{\mathbf{p}}_2^\pm)\exp(-i\mathbf{K}_2^\pm \cdot \vec{r}) \qquad (15)$$

traveling toward the bottom interface with propagation vectors $\mathbf{K}_2^\pm = k_0 n_\pm(0, -\cos\theta^\pm, \sin\theta^\pm)$. The caret in Eqs.(14) and (15) denotes a unit vector and $\hat{\mathbf{s}} = \hat{\mathbf{x}}$, $\hat{\mathbf{p}}_{1,2}^\pm = \hat{\mathbf{K}}_{1,2}^\pm \times \hat{\mathbf{x}}$.

The vector functions $\mathbf{F}^\pm$ are related to these circularly polarized waves by

$$\mathbf{F}^\pm = \tfrac{1}{2}\left(\mathbf{\Phi}_1^\pm + \mathbf{\Phi}_2^\pm\right). \qquad (16)$$

The boundary conditions requiring continuity of the tangential components of $\mathbf{E}$ and $\mathbf{H}$ at the top and bottom interfaces give rise to 8 equations, which for completeness are given in the Appendix. Using trig identities, Eqs.(A9) to (A12) can be written as linear equations for $B^\pm\sin\phi^\pm$, $B^\pm\cos\phi^\pm$ in the form

$$\mathbf{M}_\gamma(n_{eff})\begin{pmatrix} B^+ \sin\phi^+ \\ B^+ \cos\phi^+ \\ B^- \sin\phi^- \\ B^- \cos\phi^- \end{pmatrix} = 0 ,$$

$$\mathbf{M}_\gamma(n_{eff}) = \begin{bmatrix} \sigma_0^+ & -1 & \sigma_0^- & -1 \\ r_0\sigma_0^+ & -1 & -r_0\sigma_0^- & 1 \\ C^+ & -S^+ & C^- & -S^- \\ Cr^+ & -Sr^+ & -Cr^- & Sr^- \end{bmatrix} \qquad (17)$$

where

2

$$C^{\pm} = \sigma_s^{\pm} \cos(u^{\pm}d) + \sin(u^{\pm}d) \; ,$$

$$Cr^{\pm} = r_s \sigma_s^{\pm} \cos(u^{\pm}d) + \sin(u^{\pm}d) \; ,$$

$$S^{\pm} = \sigma_s^{\pm} \sin(u^{\pm}d) - \cos(u^{\pm}d) \; ,$$

$$Sr^{\pm} = r_s \sigma_s^{\pm} \sin(u^{\pm}d) - \cos(u^{\pm}d) \; , \qquad (18)$$

$$\sigma_0^{\pm} = (1 \pm \delta)\frac{u^{\pm}}{v} \; , \qquad \sigma_s^{\pm} = (1 \pm \delta)\frac{u^{\pm}}{w} \; ,$$

$$r_0 = \frac{n_0^2}{n_g^2} \; , \text{ and } r_s = \frac{n_s^2}{n_g^2} \; .$$

As usual, the vanishing of the determinant of the coefficient matrix in Eq.(17), viz.,

$$D_\gamma(n_{eff}) = \left| \mathbf{M}_\gamma(n_{eff}) \right| = 0 \; , \qquad (19)$$

determines the effective indices n_{eff} for the allowed modes. It is instructive to note that in the limit of zero chirality the matrix M_γ can be reduced to block form and the determinant

$$D_\gamma(n_{eff}) \Big|_{\gamma=0} \equiv D_0(n_{eff}) \text{ reduces to}$$

$$D_0(n_{eff}) = 4 |\mathbf{M}_{TE}| \|\mathbf{M}_{TM}| \; , \qquad (20)$$

where

$$\mathbf{M}_{TE} = \begin{bmatrix} \sigma_0 & -1 \\ C & -S \end{bmatrix} , \quad \mathbf{M}_{TM} = \begin{bmatrix} r_0\sigma_0 & -1 \\ Cr & -Sr \end{bmatrix} . \qquad (21)$$

The matrix elements in Eq.(21) are devoid of $\pm$ superscripts and correspond to the respective quantities defined in Eq.(18) but with $\gamma=0$. The separate vanishing of the determinants in Eq.(20) gives rise to the well-known[22] TE and TM mode equations, which will be further discussed below.

Eq.(19) only yields the allowed effective indices n_{eff}. To determine the remaining parameters, as well as an alternate approach to determining n_{eff} we return to Eqs. (A9-A12) and require the vanishing of the determinant of the coefficients of B^+ and B^- in Eq.(A9) taken with (A10) and of the determinant of the coefficients of B^+ and B^- in Eq.(11) taken with (12). After some algebraic manipulation, we can write these conditions in the respective forms

$$\frac{1}{1 - \dfrac{\cot(\phi^+)}{\sigma_0^+}} + \frac{1}{1 - \dfrac{\cot(\phi^-)}{\sigma_0^-}} = \frac{1}{\Delta_0} \; , \qquad (22)$$

and

$$\frac{1}{1 - \dfrac{\cot(u^+d - \phi^+)}{\sigma_s^+}} + \frac{1}{1 - \dfrac{\cot(u^-d - \phi^-)}{\sigma_s^-}} = \frac{1}{\Delta_s} \; , \qquad (23)$$

where $\Delta_0 = \frac{1}{2}(1 - r_0)$ and $\Delta_s = \frac{1}{2}(1 - r_s)$. These equations are identically satisfied upon introduction of new parameters g and h such that

$$\cot(\phi^{\pm}) = \sigma_0^{\pm}\left(\frac{r_0 \pm g}{1 \pm g}\right) \; , \qquad (24)$$

and

$$\cot(u^{\pm}d - \phi^{\pm}) = \sigma_s^{\pm}\left(\frac{r_s \pm h}{1 \pm h}\right) . \qquad (25)$$

As a consequence, Eqs.(24) reduce Eqs.(A9) and (A10) to the single equation

$$B^+ \frac{\sigma_0^+ \sin\phi^+}{1+g} + B^- \frac{\sigma_0^- \sin\phi^-}{1-g} = 0 \; , \qquad (26)$$

and Eqs.(25) reduce Eqs.(A11) and (A12) to the single equation

$$B^+ \frac{\sigma_s^+ \sin(u^+d - \phi^+)}{1+h} + B^- \frac{\sigma_s^- \sin(u^-d - \phi^-)}{1-h} = 0 \; . \qquad (27)$$

Requiring the determinant of the coefficients of B^+ and B^- to vanish in Eqs.(26)-(27) gives another condition that can be written

$$\left(\frac{1+h}{1-h}\right) = \frac{Sr_0^+ + S_0^+ g}{Sr_0^- - S_0^- g} \; ,$$

$$\qquad\qquad (28)$$

$$S_0^{\pm} \equiv \sigma_0^{\pm}\sin(u^{\pm}d) - \cos(u^{\pm}d) \; ,$$

$$Sr_0^{\pm} \equiv r_0\sigma_0^{\pm}\sin(u^{\pm}d) - \cos(u^{\pm}d) \; ,$$

where we have used trig identities and Eqs.(24) together with $\sigma_0^+ \sigma_s^- = \sigma_s^+ \sigma_0^-$, which follows from their definitions in Eqs.(18). Eqs.(24),(25) and (28) represent five equations for the 5 unknowns $\phi^{\pm}$, g, h, and n_{eff} and contain all conditions on these parameters imposed by the boundary conditions.

Equations for the subset (g, n_{eff}) can be obtained by eliminating $\phi^{\pm}$ in Eqs.(24) and (25) and also solving (28) for h as a function of g to arrive at

$$u^{\pm}d = \cot^{-1}\left(\sigma_0^{\pm}\frac{r_0 \pm g}{1 \pm g}\right) + \cot^{-1}\left(\sigma_s^{\pm}\frac{r_s \pm h}{1 \pm h}\right) + m^{\pm}\pi \; , \qquad (29)$$

$$h(g, n_{eff}) = \frac{(Sr_0^+ - Sr_0^-) + (S_0^+ + S_0^-)g}{(Sr_0^+ + Sr_0^-) + (S_0^+ - S_0^-)g} \; , \qquad (30).$$

where $m^{\pm}$ are integers that are not necessarily equal. Using Eq.(30), the two equations in (29) can be simultaneously solved[23] for g and n_{eff} after which the phases $\phi^{\pm}$ can then be found from (24). Eqs.(29) reduce to the equation[24] for the TM modes of achiral media in the limits ($\gamma\rightarrow0$, $g\rightarrow0$) $\Rightarrow$ $h\rightarrow0$, although it also has solutions with TE mode limits as $\gamma\rightarrow0$ as explained in the following text. For each value of m in Eq.(29) there are two solutions for n_{eff}: one with $|g| \leq 1$ and one with $|g| > 1$. The former has the above-mentioned TM mode limit for $\gamma\rightarrow0$, while the latter has a TE mode limit for $\gamma\rightarrow0$. Formally, the TE mode

limit of Eqs.(29) and (30) is $(\gamma\rightarrow 0,\ g\rightarrow\pm\infty)\Rightarrow h\rightarrow\pm\infty$. Because efficient numerical solution of Eq.(29) requires good initial guesses for the unknowns n_{eff} and g, it is advantageous for the modes with a TE limit (*viz.*, those with $|g|>1$) to change to new parameters

$$\bar{g}=1/g,\qquad \bar{h}=1/h, \qquad (31)$$

in order to limit the parameter space in which to search for a solution. With these substitutions, Eqs.(29) and (30) take the forms

$$u^{\pm}d=\cot^{-1}\left(\sigma_0^{\pm}\frac{r_0\,\bar{g}\pm 1}{\bar{g}\pm 1}\right)+\cot^{-1}\left(\sigma_s^{\pm}\frac{r_s\,\bar{h}\pm 1}{\bar{h}\pm 1}\right)+m^{\pm}\pi \quad, \quad (32)$$

$$\bar{h}(\bar{g},n_{eff})=\frac{(Sr_0^{+}+Sr_0^{-})\bar{g}+(S_0^{+}-S_0^{-})}{(Sr_0^{+}-Sr_0^{-})\bar{g}+(S_0^{+}+S_0^{-})}, \qquad (33)$$

and the parameter space for solutions with a TE mode limit is then restricted to $|\bar{g}|\le 1$. In both cases, values of n_{eff} are limited to $\max(n_0,n_s)<n_{eff}<\min(n_+,n_-)$ if both the RHC and LHC components of the modes [see Eqs. (14)-(16)] are to be totally internally reflected as required for completely guided modes. Once n_{eff} and g (or $\bar{g}$) are found, the phases $\phi^{\pm}$ can be obtained from Eq.(24) and, selecting B^{-} as the arbitrary amplitude, the remaining constants $A^{\pm}$, B^{+}, and $C^{\pm}$ can be obtained from Eqs.(26), (30), (A1-A2), and (A5-A6):

$$B^{+}=B^{-}\left(\frac{g+r_0}{g-r_0}\right)\frac{\cos\phi^{-}}{\cos\phi^{+}}, \qquad (34)$$

$$A^{\pm}=B^{-}\cos\phi^{-}\left(\frac{g\pm\sqrt{r_0}}{g-r_0}\right), \qquad (35)$$

$$C^{\pm}=B^{-}\cos\left(u^{-}d-\phi^{-}\right)\left(\frac{h\pm\sqrt{r_s}}{h-r_s}\right). \qquad (36)$$

Note that for modes involving solutions $\bar{g}$ of Eq.(32), the phases $\phi^{\pm}$, and constants $A^{\pm}$, B^{+}, and $C^{\pm}$ can be found from Eqs.(24) and (34-36) simply by first calculating the corresponding value of g using $g=1/\bar{g}$.

4. DISCUSSION

Polarization of the Transverse Electric Field

An essential step leading to the form of the solution to the chiral core asymmetric planar waveguide given in the previous section is recognizing that two of the constraints arising from the boundary conditions can be written in the particular forms given in Eqs.(22) and (23), which can then readily be seen to be identically satisfied by introduction of the parameters g and h as in Eqs.(24) and (25). We will now show that these

parameters (as well as their counterparts $\bar{g}$ and $\bar{h}$) are measures of the eccentricity of the polarization ellipse for the transverse electric field in the top and bottom claddings.

From Eqs.(3), (8), and (9), the transverse electric field is given by

$$\mathbf{E}_T=\frac{1}{2}\left\{[\psi^{+}(y)+\psi^{-}(y)]\hat{\mathbf{x}}+in_{eff}\left[\frac{\psi^{+}(y)}{n_{+}}-\frac{\psi^{-}(y)}{n_{-}}\right]\hat{\mathbf{y}}\right\}$$

$$\times\,\exp(-ik_0 n_{eff}z)$$

$$(37)$$

which is recognized to be elliptically polarized in general, with major axes lying along either the *x*- or *y*-axes. Using Eq.(35) in (37), the ratio of the *y*-component to the *x*-component everywhere in the top cladding (achiral) is given by

$$\left.\frac{E_y}{E_x}\right|_{y\ge 0}=i\frac{n_{eff}}{n_0}\frac{\sqrt{r_0}}{g}=i\frac{n_{eff}}{n_g}\frac{1}{g}. \qquad (38)$$

Noting that $n_{eff}/n_g\approx 1$, especially far from cutoff, the polarization state of the transverse field in the top cladding can be inferred from the value of g as follows:

TM: $\qquad g\rightarrow 0$

TE: $\qquad g\rightarrow\pm\infty$ (or $\bar{g}\rightarrow 0$)

~RHC: $\qquad g\rightarrow +1$ (or $\bar{g}\rightarrow +1$)

~LHC: $\qquad g\rightarrow -1$ (or $\bar{g}\rightarrow -1$)

$$(39)$$

The parameter h gives the polarization state of the transverse field in the bottom cladding in a similar fashion because the use of Eq.(36) in (37) gives

$$\left.\frac{E_y}{E_x}\right|_{y\le -d}=i\frac{n_{eff}}{n_s}\frac{\sqrt{r_s}}{h}=i\frac{n_{eff}}{n_g}\frac{1}{h}. \qquad (40)$$

In the core, the eccentricity of the polarization ellipse varies as a function of *y*. The polarization state there is seen to depend on B^{+} and B^{-} as follows: $B^{-}=0\Rightarrow$ RHC, $B^{+}=0\Rightarrow$ LHC, $[B^{-}\rightarrow B^{+}$ as $\gamma\rightarrow 0]\Rightarrow$ TE, $[B^{-}\rightarrow -B^{+}$ as $\gamma\rightarrow 0]\Rightarrow$ TM. From Eqs.(24) and (26), we can derive the equation

$$\frac{B^{+}}{B^{-}}=sign\left[\frac{(g+1)}{(g-1)}\right]$$

$$\times\sqrt{\left\{\left[\frac{(g+1)}{\sigma_0^{+}}\right]^2+(g+r_0)^2\right\}\bigg/\left\{\left[\frac{(g-1)}{\sigma_0^{-}}\right]^2+(g-r_0)^2\right\}}$$
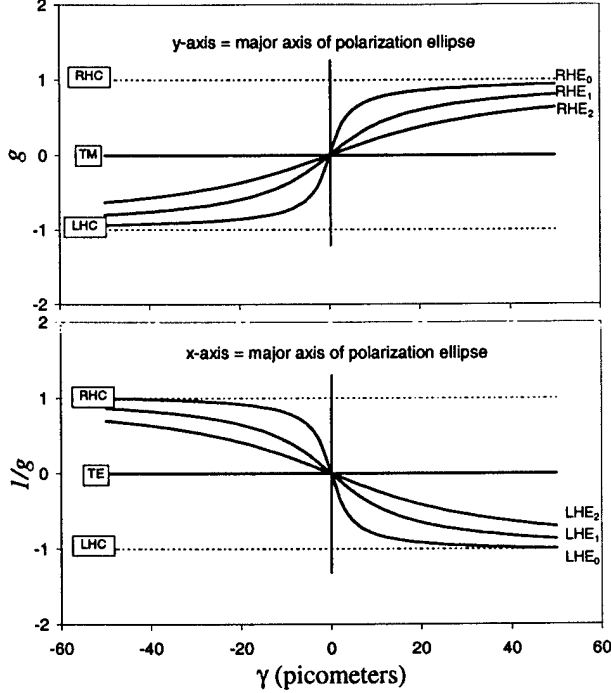
$$(41)$$

4

Figure 2. Plots of the eccentricity parameter g versus chirality for the first six elliptical modes in a planar waveguide with a 3 μm thick core and $n_g = 1.59$, $n_0 = 1.00$, $n_s = 1.51$. Top plot: modes that are RH elliptical for $\gamma > 0$ (and LH elliptical for $\gamma < 0$) evolving from TM modes at $\gamma = 0$. Bottom plot: modes that are LH elliptical for $\gamma > 0$ (and RH elliptical for $\gamma < 0$) evolving from TE modes at $\gamma = 0$.

which relates the polarization state in the core to the parameter g. In the limit of zero chirality, in which case $\sigma_0^- \rightarrow \sigma_0^+$, the TE and TM mode limits are obtained for $g \rightarrow \pm\infty$ ($\overline{g} \rightarrow 0$) and $g \rightarrow 0$, respectively. For the allowed modes in a chiral core waveguide, the transverse electric field is elliptically polarized. When the amount of chirality is small (as discussed more fully later), the modes are nearly TE (or TM) because the major axis is much larger than the minor axis. Modes with a predominant RHC polarization or LHC polarization are realized when $g \rightarrow \pm1$, as can be seen from Eq.(41). There is a maximum on the right-hand side of Eq.(41) as $g \rightarrow 1$, so that $B^+/B^- \gg 1$ resulting in predominantly RHC polarization, and a minimum as $g \rightarrow -1$, so that $B^+/B^- \ll 1$ resulting in predominantly LHC polarization.

Polarization Dependence on Chirality

In an achiral film, as is well known, the modes are transverse electric (TE) and transverse magnetic (TM). An example of the transition with increasing chirality from TE/TM modes in the achiral case to predominantly right- and left-handed circularly polarized modes is demonstrated in Figure 2 for a planar waveguide with a 3 μm thick core and $n_g = 1.59$, $n_0 = 1.00$, $n_s = 1.51$. These values are illustrative of a chiral polymer on a glass substrate at a wavelength of 633nm. The parameter g, which is proportional to the eccentricity of the polarization
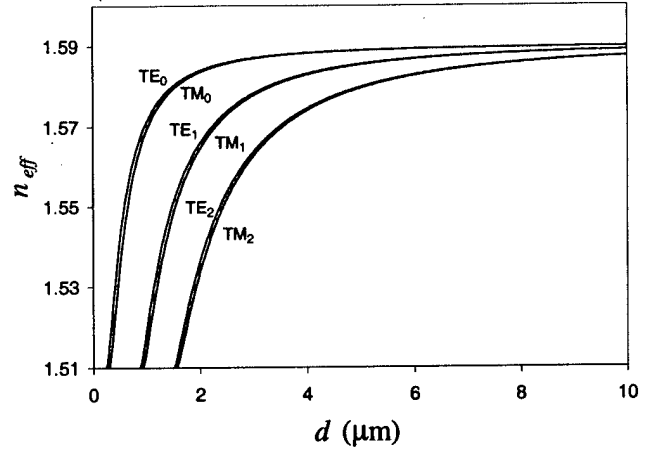

Figure 3. Effective index n_{eff} vs thickness d curves for TE and TM modes in an achiral ($\gamma = 0$) asymmetric planar waveguide with $n_g = 1.59$, $n_0 = 1.00$, $n_s = 1.51$.

ellipse, is plotted versus the chirality parameter γ for the first six elliptical modes. The top plot shows the modes that are RH elliptical for $\gamma > 0$ (and LH elliptical for $\gamma < 0$) evolving from TM modes at $\gamma = 0$, and the bottom plot shows the modes that are LH elliptical for $\gamma > 0$ (and RH elliptical for $\gamma < 0$) evolving from TE modes at $\gamma = 0$. For convenience, the curves are labeled according to the handedness of the mode for positive γ. These curves are solutions of Eqs.(29) and (30) for the case $|g| \leq 1$, and Eqs.(32) and (33) for $|g| > 1$. The horizontal dotted lines identify the values $g = +1$ and $g = -1$ corresponding to predominantly RHC and LHC polarization, respectively, of the transverse electric field. Note that for a given chirality, the higher the order the more elliptical (less circular) are the modes. The polarization eccentricity for a given elliptical mode also depends on the core thickness, as discussed in the next section.

Thickness dependence and cutoff conditions

Figures 3 and 4 show the mode effective index as a function of increasing film thickness for an achiral ($\gamma = 0$) and a chiral ($\gamma = 4.5 \times 10^{-5}$ μm) waveguide, respectively. In the well-known case of the achiral waveguide (Figure 3), note that the effective indices for TE and TM modes of a given order get closer together as the thickness increases and there are no crossover points. In the chiral waveguide (Figure 4), on the other hand, the right-handed elliptical (RHE) and left-handed elliptical (LHE) modes of a given order separate as the core gets thicker and the RHE modes cross over LHE modes at numerous thickness values, as shown more clearly in the inset in Figure 4. In addition to the usual cutoff at a minimum thickness, the LHE modes all experience a second cutoff with increasing thickness determined by the chirality and refractive indices. This mode separation and mode crossover with increasing thickness were also found in the derivations in Refs. 12 and 18, but neither of these previous works discussed the existence of the second cutoff for completely guided LHE modes.

Just like the achiral case, the cutoff at minimum thickness for the LHE and RHE modes occurs when n_{eff} is at its minimum value, i.e., the larger of n_0 and n_s. Assuming $n_0 < n_s$, the cutoff thickness is found by simultaneously solving for the cutoff
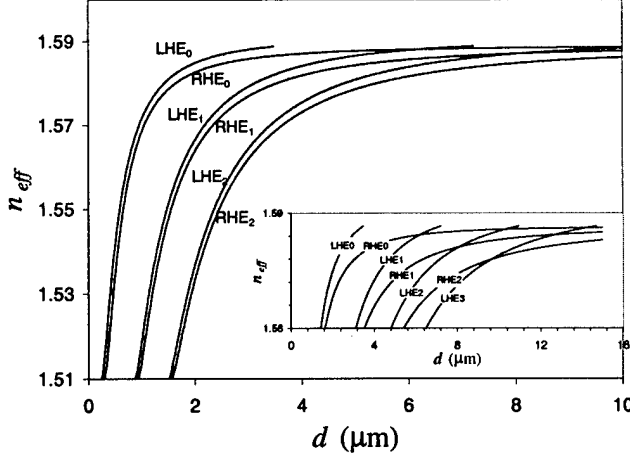
5

Figure 4. Effective index n_{eff} vs thickness d curves for RHE and LHE modes in a chiral ($\gamma = 45\ pm$) asymmetric planar waveguide with $n_g = 1.59$, $n_0 = 1.00$, $n_s = 1.51$. The inset is a blowup emphasizing the mode crossover points and second cutoff of the LHE modes.
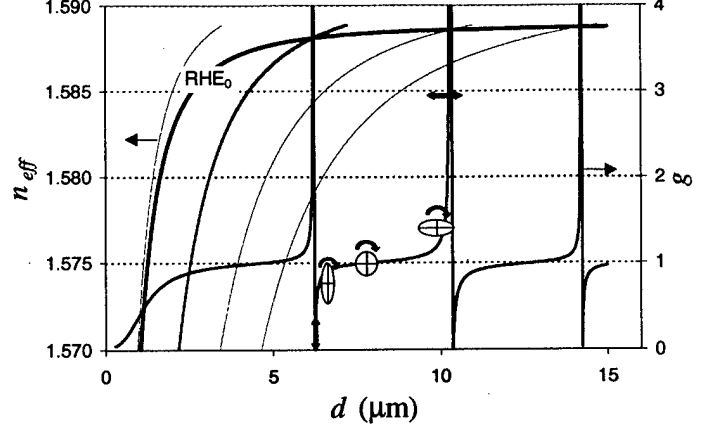

Figure 5. A plot of the effective index (left axis) and eccentricity parameter g (right axis) for the RHE$_0$ mode versus thickness illustrating the variation in eccentricity in the vicinity of the intersections of the RHE$_0$ mode effect index (left axis) with the LHE modes (faint lines) for the same waveguide parameters as in Figure 4. The icons included to help visualize the eccentricity are: vertical double arrow – TM, horizontal double arrow – TE, ellipses – elliptical polarization with x or y major axis.

values g_c and d_c with $n_{eff} = n_s$ substituted in the two equations (29). (Because arccot (∞) = 0, the equations do not contain h_c.) These equations can be conveniently solved in two steps. First, g_c is found as the root of

$$u_c^+ (\phi_c^- + M\pi) - u_c^- (\phi_c^+ + M\pi) = 0 \ , \qquad (42)$$

where

$$u_c^\pm = k_0 \sqrt{(n^\pm)^2 - n_s^2} \ ,$$

$$\phi_c^\pm = \cot^{-1}\left[(1 \pm \delta) \sqrt{\frac{(n^\pm)^2 - n_s^2}{n_s^2 - n_0^2}} \frac{r_0 \pm g_c}{1 \pm g_c} \right] , \qquad (43)$$

and M represents the mode number M^+ for RHE or M^- for LHE modes. Once g_c is found, the cutoff thickness at a given wavelength can then be obtained from

$$k_0 d_c = \frac{\phi_c^\pm + M^\pm \pi}{\sqrt{(n^\pm)^2 - n_s^2}} . \qquad (44)$$

The cutoff value h_c is given by

$$h_c = r_s \left\{ 1 - 2\left[\frac{\cos(u_c^- d_c)(r_0 + g_c)}{\cos(u_c^+ d_c)(r_0 - g_c)} + 1 \right]^{-1} \right\} . \qquad (45)$$

In Eqs. (42)-(45), the ranges of solutions for g_c are

$\gamma > 0$:

RHE$(M=M^+) \Rightarrow 0 < g_c \leq 1$, LHE$(M=M^-) \Rightarrow -\infty < g_c < -r_0$
$\gamma < 0$:
RHE$(M=M^+) \Rightarrow r_0 < g_c < \infty$, LHE$(M=M^-) \Rightarrow -1 \leq g_c < 0$.

$$(46)$$

For those cases in Eqs.(46) where $|g_c| > 1$, it is advantageous numerically to solve instead for $\bar{g}_c$ using $\bar{\phi}_c^\pm$ in place of $\phi_c^\pm$ in Eqs.(42) and (44), where $\bar{\phi}_c^\pm$ has the same definition as $\phi_c^\pm$ in Eq.(43) but with g_c replaced by $1/\bar{g}_c$.

The second cutoff at maximum thickness for LHE modes (RHE modes when $\gamma < 0$) arises because both of the equations (corresponding to the two signs) in Eq.(32) must be satisfied simultaneously for a given mode and the maximum real value of n_{eff} for completely guided modes is $n_{eff} = n^+$ (when $\gamma > 0$).[25] No matter how dominant one handedness of circularly polarized waves becomes over the other handedness, both types of waves must be present in order to satisfy the boundary conditions. [Recall that both LHE and RHE waveguide modes are comprised of the total field from two RHC-polarized waves and two LHC-polarized waves, as in Eqs.(14) and (15), and $n^\pm$ are the refractive indices associated with these waves.] Thus, even for LHE modes u^+ must be real, which requires that $n_{eff} < n^+$.
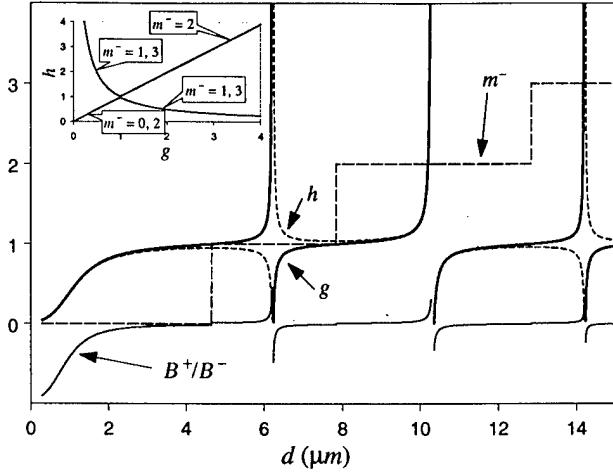
Figure 6. Relationship of the substrate eccentricity parameter h (short-dashed line) to the upper cladding eccentricity parameter g (solid line) as a function of thickness for the RHE_0 mode of Figures 4 and 5. The inset shows $h \approx g$ when $m^- - m^+$ is even and $h \approx 1/g$ when $m^- - m^+$ is odd. Also shown for reference is the core amplitude ratio B^+/B^- versus thickness.

Noting that the cutoff here occurs also with nearly circular polarization, we put $n_{eff} = n^+$ together with $g = h = -1$ in Eq.(32) to obtain

$$d_{c2}(M^-) = \left\{ \cot^{-1}\left[(1-\delta)\sqrt{\frac{(n^-)^2-(n^+)^2}{(n^+)^2-n_0^2}} \frac{r_0+1}{2} \right] \right.$$

$$+ \cot^{-1}\left[(1-\delta)\sqrt{\frac{(n^-)^2-(n^+)^2}{(n^+)^2-n_s^2}} \frac{r_s+1}{2} \right] \quad (47)$$

$$\left. + M^-\pi \right\} \Big/ k_0\sqrt{(n^-)^2-(n^+)^2}$$

Because $\delta \ll 1$, an approximate value for this cutoff thickness is given by

$$d_{c2}(M^-) \approx \frac{1}{2k_0 n_g}\left[\frac{(M^-+1)}{\sqrt{\delta}}\pi - \left(\frac{1+r_0}{\sqrt{1-r_0}} + \frac{1+r_s}{\sqrt{1-r_s}} \right) \right]. \quad (48)$$

From this expression it can be seen that in the achiral limit (whence $\delta \to 0$), this second cutoff thickness becomes infinite, consistent with the nonexistence of such a second cutoff in the achiral case. The maximum thickness cutoff of the LHE_0 mode for the example in Figure 4, which has $\gamma=4.5\times10^{-5}$ μm, occurs at slightly less than 3 μm. This value of γ corresponds to a bulk rotatory power of 642 deg/mm at a wavelength of 633nm. For reference, a bulk rotatory power of 30 deg/mm ($\gamma=2.1\times10^{-6}$ μm)
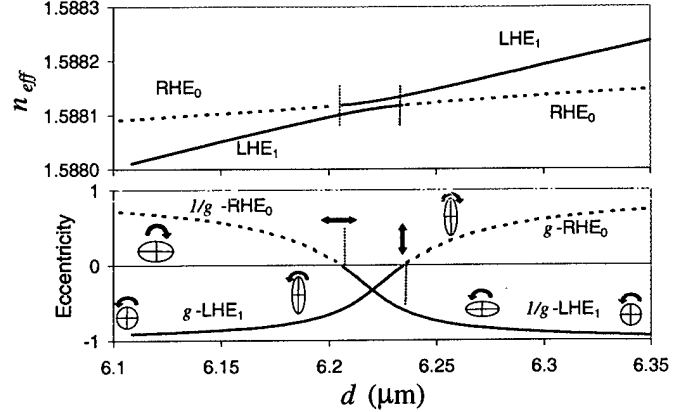

Figure 7. Detail of the crossover of mode RHE_0 (dotted line) with LHE_1 (solid line) in Figures 4-6. Top plot: effective indices versus thickness. Bottom plot: eccentricity parameter g for RH polarization ($1/g$ for LH polarization) versus thickness. In the narrow transition region, indicated by vertical dotted lines, only LH polarization exists.

results in a maximum thickness cutoff of 16.7 μm for the LHE_0 mode.

At this point, we note the connection between our solutions and the approximate solutions for the asymmetric planar waveguide given in Ref. 18. We can obtain the RHC mode equations of their work by putting $g=1$, $h=1$, $r_s=1$, and solve Eq.(29) with the plus sign while ignoring the corresponding equation with a minus sign. Similarly, their LHC modes can be obtained by setting $g=-1$, $h=-1$, $r_s=1$ and solve Eq.(29) with the minus sign while ignoring the companion equation with a plus sign. This gives reasonably good values for the effective indices of the RH-modes in general and for the LH modes between the low and high thickness cutoff values. However, the approximations used in Ref. 18 resulted in missing the second thickness cutoff for the LHE modes ($\gamma>0$) and ignoring the fact that higher order modes have differing degrees of elliptical polarization (see Figure 2).

Eccentricity and mode crossover points

In this section we examine the behavior of mode eccentricity with increasing thickness, the relationship between the integers $m^{\pm}$ and the mode order numbers $M^{\pm}$, and the details of the mode crossover points. In Figure 5 is plotted the effective index (left axis) for the RHE_0 mode along with the eccentricity parameter g (right axis) as a function of thickness. With increasing thickness d, the effective index n_{eff} for RHE_0 crosses over successively higher LHE modes, viz., LHE_1, LHE_2, etc. To obtain this curve for mode $M^+=0$, Eqs.(29) and (30) are solved, starting from cutoff, with $m^+ = 0$ and, initially, $m^- = 0$. The eccentricity parameter g for the upper cladding starts out small in this example (nearly TM, with the y-axis the major axis of the polarization ellipse) but increases to $g = 1$ (circular polarization) as d increases. There is then a π discontinuity in arccot and m^- increases by 1 to $m^- = 1$. With further increase in thickness, the x-axis becomes the major polarization axis (because $g >1$) and eventually $g \to\infty$ (TE) as RHE_0 crosses over LHE_1. After
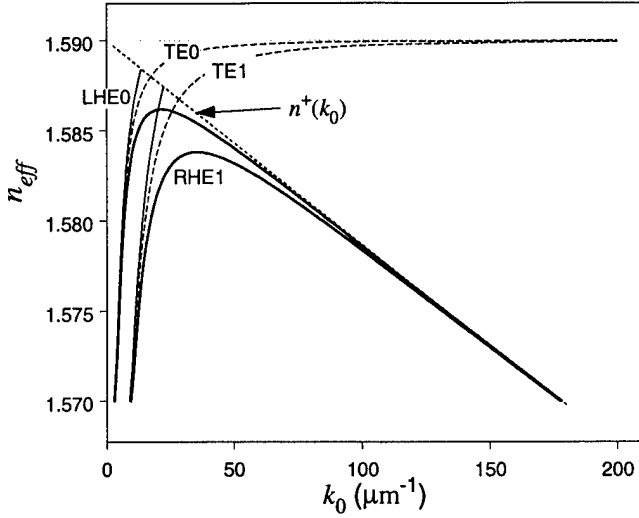
Figure 8. Effective index n_{eff} vs. thickness k_0 mode curves for a 2 μm thick core with $n_g = 1.59$, $n_0 = 1.00$, and $n_s = 1.57$. The LHE modes are cut off by the line $n_{eff} = n^+(k_0)$, while the RHE modes are asymptotic to this line undergoing a high frequency cutoff when $n^+(k_0) \to n_s$.
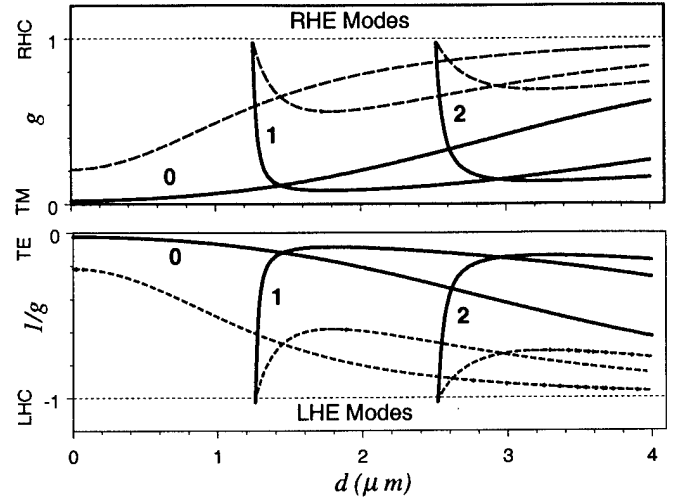
Figure 9. Eccentricity parameter g for the first three RHE modes (top plot) and $1/g$ for the first three LHE modes (bottom plot) versus thickness for chirality $\gamma=0.45$ picometers (solid line) and $\gamma=4.5$ picometers (dotted line) in a symmetric waveguide with $n_g = 1.59$ and $n_0 = n_s = 1.57$. The values at cutoff [see Eq.(52)] for all but the zeroth order modes are $g_c = \pm r_s$, where, in this example, $r_s = 0.975$; note the initial rapid falloff and subsequent rise for $d>d_c$.

crossing over LHE$_1$, the sequence repeats, starting with $g = 0$ (TM), then RH elliptical with major y-axis, increasing to $g = 1$ (circular, where m^- is bumped up to $m^- = 2$), then RH elliptical with major x-axis, and finally g $\to\infty$ (TE) as the LHE$_2$ crossover approaches. Polarization ellipse icons are included in Figure 5 to help visualize this sequence. In general, for an RHE mode M^+, we fix $m^+ = M^+$ in Eqs.(29) and (30) [or Eqs.(32) and (33)] and m^- varies according to $m^- = M^+$, $M^+ + 1$, $M^+ + 2$, ... with increasing d.

The polarization parameter h, which is proportional to the eccentricity in the substrate, satisfies $h \approx g$ when $m^- - m^+$ is an even integer, and $h \approx 1/g$ when $m^- - m^+$ is an odd integer. This is shown in Figure 6, where h, g, m^-, and B^+/B^-, are plotted versus thickness for the RHE$_0$ mode. The inset shows h plotted directly against g .

A similar sequence of events occurs for the LHE modes with the differences that now g is negative and a given LHE mode only crosses over RHE modes of lower mode number as the thickness increases. In general, for LHE mode M^-, we fix $m^- = M^-$ and m^+ varies according to $m^+ = M^-$, $M^- - 1$, $M^- - 2$, ... , -1 with increasing thickness, with cutoff occurring while $m^+ = -1$.

It would seem that there is an abrupt polarization discontinuity at the cross-over points in Figure 5. However, on closer examination, it turns out that there is a transition region at the mode crossovers, as illustrated in Figure 7 with vertical dotted lines for the RHE$_0$/LHE$_1$ crossover. Inside this small region, both modes are LH elliptical – one with an x-major axis and one with a y-major axis. The effective index curve for RHE$_0$ merges continuously from the left into the LHE$_1$ curve, and the eccentricity for RHE$_0$ varies continuously from RH elliptical, with x-major axis, to TE ($1/g=0$), to LH elliptical with x-major axis. The effective index curve for LHE$_1$ merges continuously from the left into the RHE$_0$ curve, and the eccentricity for LHE$_1$ varies continuously from LH elliptical, with y-major axis, to TM ($g=0$), to RH elliptical with y-major axis. Although this behavior

contradicts, somewhat, the designation RHE inside this region, we maintain the RHE/LHE mode designations because the crossover transition regions are very small.

In general, the thickness values for the transition region edges for the RHE$_{M^+}$ mode at the LHE$_{M^-}$ crossover region can be obtained from Eqs.(29) using

$M^- - M^+ =$ odd integer
  low-d side: $1/g = 0$, $h = 0$
  high-d side: $g = 0$, $1/h = 0$;

(49)

$M^- - M^+ =$ even integer
  low-d side: $1/g = 0$, $1/h = 0$
  high-d side: $g = 0$, $h = 0$.

These substitutions in Eq.(29), together with $m^- = M^-$ and $m^+ = M^+$, yield two equations with unknowns n_{eff} and d. They can be straightforwardly solved by first eliminating d, solving the resulting equation numerically for n_{eff}, and then using either of the original equations to find d.

Frequency dependence

Ref. 18 predicted two frequency cutoff values for the right-handed modes.[26] We will show that both RHE and LHE modes have a low-frequency and a high-frequency cutoff for completely guided modes, although for different reasons. The low frequency cutoff is the usual one that corresponds to the maximum wavelength λ_c for which a waveguide of given thickness d can still support the mode $M^\pm$ of interest. This can be found by simultaneously solving for the cutoff values $k_{0c} = 2\pi/\lambda_c$ and g_c in the two equations

$$u_c^{\pm} d = \phi_c^{\pm} + m^{\pm} \pi , \qquad (50)$$

where $u_c^{\pm}$ and $\phi_c^{\pm}$ are given by Eqs.(43), taking into account that $\delta = k_0 n_g \gamma$ and $n^{\pm} = n_g /(1 \pm \delta)$ are wavelength dependent. At this cutoff we put $m^+ = m^- = M^+$ for RHE modes and $m^+ = m^- = M^-$ for LHE modes.

Starting from these cutoff values, Figure 8 shows the effective index for the first two LHE and RHE modes plotted as a function of $k_0 = 2\pi/\lambda$ for a 2 μm thick core with $n_g = 1.59$, $n_0 = 1.00$, and $n_s = 1.57$. In the interest of simplicity, the frequency dependence of the chirality parameter γ and of the average index n_g is not taken into account in this plot. For reference, the frequency dependence of the effective index for the first two TE modes are plotted for the achiral guide with a core index of n_g. (The TM modes are virtually indistinguishable from the TE modes on this scale.) Just as there is a maximum thickness cutoff for completely guided LHE modes, there is a high frequency cutoff that occurs as $n_{eff} \to n^+(k_0)$ for these modes. The numerical value can be obtained by finding the root k_{0c2} that satisfies Eq.(48) [after replacing d_{c2} with the desired thickness d] together with (6). The corresponding left-handed polarized modes in Ref. 18 have no high frequency cutoff and continue indefinitely with increasing k_0.

A high frequency cutoff for the right-handed modes[18] seen in Figure 8 arises because in order for completely guided modes to exist the effective index is limited to $n_s < n_{eff} < n^+$

(here assuming $\gamma > 0$ and $n_s > n_0$). As $n^+ = n_g /(1 + \delta)$ decreases with increasing δ (decreasing λ), there will be some sufficiently short wavelength such that the limit $n^+ \to n_s \Rightarrow \delta \approx (1 - r_s)/2$ is reached, and no guided modes are allowed.

The eccentricity parameter g also undergoes dramatic changes as a function of frequency at a fixed thickness, like those changes shown in Figs. (5) and (6) for the case of changing thickness and fixed frequency.

The symmetric chiral-core planar waveguide

As the refractive index n_0 of the upper cladding approaches n_s for the lower cladding, the ranges of thickness values where $m^- - m^+$ is an odd integer (for example, the regions in Figure 6 where $h \approx 1/g$) become narrower and narrower until, in the limit $n_0 = n_s$, only even integer differences exist and $h = g$ everywhere. In this limit, Eq.(29) reduces to

$$u^{\pm} d = 2\phi^{\pm} + m^{\pm} \pi , \qquad (51)$$

with $\phi^{\pm}$ given by Eq.(24). [Note that Eq.(25) is now equivalent to (51)]. When Eq.(51) is solved for $\phi^{\pm}$ and substituted in Eq.(11), the solutions to Eqs.(10) in the core take the forms

$$\psi_{core}^{\pm}(y) = B^{\pm} \cos\left(u^{\pm}(y + d/2) + m^{\pm} \pi/2\right), \quad 0 < y < -d , \quad (52)$$

which are easily seen to separate into even or odd functions (viz., pure cosines or sines) depending on whether $m^{\pm}$ are even or odd

integers, respectively. As the waveguide thickness increases for RHE modes ($m^+ = M^+$), the integer m^- progresses through the series $m^- = M^+, M^+ + 2, M^+ + 4, \dots$, with the change to the next higher value occurring as g passes through +1. For the LHE modes ($m^- = M^-$), m^+ varies according to $m^+ = M^- - 2$ (for $M^- \neq 0$), $M^-, M^- - 2, M^- - 4, \dots$ with the change to the next value occurring as g passes through −1; the second cutoff at maximum thickness occurs at $m^+ = 0$ for even modes and $m^+ = -1$ for odd modes.

The cutoff at minimum thickness for the symmetric waveguide, given by Eq.(44) with $\phi_c^{\pm} \to 0$ as $n_0 \to n_s$, is the same as found in Ref. 12. As in the achiral case, the zeroth order modes persist down to $d=0$. To obtain the values of g at cutoff, we use Eq.(51) with (43) in the limit $n_{eff} \to n_s = n_0$. For the cutoff of RHE modes ($g>0$, $m^+=M^+$) we have $\phi_c^+ \to 0$ and $\phi_c^- \neq 0$, while $\phi_c^+ \neq 0$ and $\phi_c^- \to 0$ for the cutoff of LHE modes ($g<0$, $m^-=M^-$). For $\delta \neq 0$ we get

$$g_c^{\pm} = \begin{cases} -G \pm \sqrt{G^2 + r_s} , & M^{\pm} = 0 \\ \pm r_s , & M^{\pm} \neq 0 \end{cases} , \qquad (53)$$

where

$$G = \frac{\Delta_s^2}{\delta(1 - \Delta_s)} . \qquad (54)$$

It is notable that for $M^{\pm} \neq 0$, the cutoff value of the eccentricity parameter g is independent of the chirality parameter γ, so long as $\gamma \neq 0$. This is illustrated in Figure 9, which shows the behavior of g near cutoff for the first three RHE and LHE modes. In addition, as follows from Eq.(41), $B^-=0$ at an RHE cutoff and $B^+=0$ at an LHE cutoff. The second cutoff at maximum thickness for the LHE modes in the symmetric case is given by Eqs.(47) and (48) with $r_0 = r_s$.

5. CONCLUSION

In this paper we have presented the general solution in Eqs.(29) and (30) for modes in an asymmetric planar waveguide with an isotropic chiral core in terms of a pair of parameters g and h related to the eccentricity of the polarization ellipse for the transverse electric field [see Eqs.(38) and (40)]. The symmetric waveguide is discussed as a limiting case. This formulation provides insight into the transition, with increasing chirality of the core, from TE/TM modes in the achiral case to modes with nearly right-handed and left-handed circular polarization. The polarization of the transverse electric field for the modes is elliptical in general with RHE (right-handed elliptical) modes evolving from TM modes and LHE modes evolving from TE modes as the chirality parameter γ increases from zero. The eccentricity of the polarization of the transverse electric field varies dramatically with thickness and with frequency. Expressions for the minimum thickness cutoff values are given in Eqs.(42)-(44) for the asymmetric waveguide and in Eqs.(44) and (53) for the symmetric waveguide. For materials with positive γ, completely guided LHE modes (RHE modes for negative γ) experience a second thickness cutoff, given by Eq.(48), so that total internal reflection of both the RHC and LHC components of

these left-handed modes occurs only between a minimum and maximum thickness. Correspondingly, there are also minimum and maximum frequency cutoffs. Although the existence of a maximum frequency cutoff for the RHE modes has been reported earlier[18], the second cutoff conditions have heretofore not been reported for the LHE modes. The unique polarization properties of chiral waveguides discussed in this paper may lead to new and useful device designs.

Appendix: Boundary Conditions
The continuity of the tangential components of **E** and **H**, viz., E_x, E_z, H_x, and H_z at the two interfaces, $y = 0$ and $y = -d$, gives rise to a set of 8 equations – one less in number than the nine unknowns $A^{\pm}$, $B^{\pm}$, $C^{\pm}$, $\phi^{\pm}$, and n_{eff} – leaving arbitrary the overall amplitude of the lightwave. From Eqs.(3) together with (8), (9), and (11), one gets

E_x at $y=0$:

$$B^+ \cos\phi^+ + B^- \cos\phi^- = A^+ + A^- \tag{A1}$$

H_x at $y=0$:

$$B^+ \cos\phi^+ - B^- \cos\phi^- = \sqrt{r_0}\left(A^+ - A^-\right) \tag{A2}$$

E_z at $y=0$:

$$B^+ \sqrt{r_0}\,\sigma_0^+ \sin\phi^+ + B^- \sqrt{r_0}\,\sigma_0^- \sin\phi^- = A^+ - A^- \tag{A3}$$

H_z at $y=0$:

$$B^+ \sigma_0^+ \sin\phi^+ + B^- \sigma_0^- \sin\phi^- = A^+ + A^- \tag{A4}$$

E_x at $y=-d$:

$$B^+ \cos(u^+ d - \phi^+) + B^- \cos(u^- d - \phi^-) = C^+ + C^- \tag{A5}$$

H_x at $y=-d$:

$$B^+ \cos(u^+ d - \phi^+) - B^- \cos(u^- d - \phi^-) = \sqrt{r_s}\,(C^+ - C^-) \tag{A6}$$

E_z at $y=-d$:

$$B^+ \sqrt{r_s}\,\sigma_s^+ \sin(u^+ d - \phi^+) - B^- \sqrt{r_s}\,\sigma_s^- \sin(u^- d - \phi^-) = C^+ - C^- \tag{A7}$$

H_z at $y=-d$:

$$B^+ \sigma_s^+ \sin(u^+ d - \phi^+) + B^- \sigma_s^- \sin(u^- d - \phi^-) = C^+ + C^- , \tag{A8}$$

where $\sigma_0^{\pm}, \sigma_s^{\pm}, r_0$, and r_s are defined in Eq.(18).

Eliminating $A^{\pm}$ in the first four equations gives

$$B^+ (\sigma_0^+ \sin\phi^+ - \cos\phi^+) + B^- (\sigma_0^- \sin\phi^- - \cos\phi^-) = 0 \tag{A9}$$

and

$$B^+ (r_0\sigma_0^+ \sin\phi^+ - \cos\phi^+) - B^- (r_0\sigma_0^- \sin\phi^- - \cos\phi^-) = 0 , \tag{A10}$$

while elimination of $C^{\pm}$ in the last four equations gives

$$B^+ \left[\sigma_s^+ \sin(u^+ d - \phi^+) - \cos(u^+ d - \phi^+)\right] + B^- \left[\sigma_s^- \sin(u^- d - \phi^-) - \cos(u^- d - \phi^-)\right] = 0 \tag{A11}$$

and

$$B^+ \left[r_s\sigma_s^+ \sin(u^+ d - \phi^+) - \cos(u^+ d - \phi^+)\right] - B^- \left[r_s\sigma_s^- \sin(u^- d - \phi^-) - \cos(u^- d - \phi^-)\right] = 0 . \tag{A12}$$

As discussed in the body of this paper, these last four equations determine the effective indices n_{eff}, the phases $\phi^{\pm}$, and the ratio B^+/B^- .

REFERENCES

[1] D.L. Jaggard, A.R. Mickelson, and C.H. Papas, "On electromagnetic waves in chiral media," *J. Appl. Phys.* **19**, 211(1979).

[2] A. Lahtakia, V.K. Varadan, and V.V. Varadan, Time-Harmonic Electromagnetic Fields in Chiral Media , Lecture Notes in Physics Series 335 (Springer-Verlag, Berlin, 1989).

[3] N. Engheta and D.L. Jaggard, "Electromagnetic chirality and its applications," *IEEE Trans. Antennas and Propagation* **30**,6(1988).

[4] V.K. Varadan, A. Lakhtakia, and V.V. Varadan, "Propagation in a parallel plate waveguide wholly filled with a chiral medium," *J. Wave Mater. Interact.* **3**, 267(1988).

[5] N. Engheta and P. Pelet, "Modes in Chirowaveguides," *Optics Letters* **14**(11), 593(1989).

[6] P. Pelet and N. Engheta, "The Theory of Chirowaveguides," *IEEE Trans. Antennas and Propagation* **38**(1), 90(1990)

[7] L. Zhang, Y. Jiao, and C. Liang, "The dominant mode on parallel-plate chirowaveguides," *IEEE Trans. Microwave Theory and Techniques* **42**, 2009(1994).

[8] See for example, A. Yariv and P. Yeh, Optical Waves in Crystals (New York, J. Wiley and Sons, 1984), section 4.9.

[9] For a recent review, see M.M. Green, J.-W. Park, T. Sato, S. Lifson, R.L.B. Selinger, J.V. Selinger, *Angew. Chem. Int. Ed.* **38**, 3138 (1999).

[10] Highly chiral oligimers have been realized, for example, in metallocenes [T.J. Katz, A. Sadhakar, M.F. Teasley, A.M. Gilbert, W.E. Geiger, M. P. Robben, M. Wuensch, and M.D. Ward, *J. Am. Chem. Soc.* **115**, 3182(1993).] but additional requirements of low optical loss and incorporation into polymers with good film-forming properties must be met.

[11] M. Chien, Y. Kim, and H. Grebel, "Mode conversion in optically active and isotropic waveguides," *Optics Letters* **14**, 826(1989).

[12] M. Oksanen, P.K. Loivisto, and L.V. Lindell, "Dispersion curves and fields for a chiral slab waveguide," *IEE Proc.-H* **138**(4), 327(1991).

[13] J. Xiao, K. Zhang, and L. Gong, "Field Analysis of a General Chiral Planar Waveguide," *Int. J. of Infrared and Millimeter Waves* **18**(4), 939(1997)

[14] S.F. Mahmoud, "Guided Modes on Open Chirowaveguides," *IEEE Trans. Microwave Theory Technol.*, **MTT-43**, 205 (1995).

[15] K.M. Flood and D.L. Jaggard, "Single-mode operation in symmetric planar waveguides using isotropic chiral media," *Optics Letters* **21**, 474(1996)

[16] S. Yamamoto, Y. Koyamada, T. Makimoto, "Normal-mode analysis of anisotropic and gyrotropic thin-film devices for integrated optics," *J. Appl. Phys.* **43**, 5090(1972).

[17] P.Pelet and N. Engheta, "Coupled-mode theory for chiral waveguides," *J. Appl. Phys.* **67**,2742(1990).

[18] S.V. Demidov, K.V. Kushnarev, and V.V. Shevchenko, "Dispersion Properties of the Modes of Chiral Planar Optical Waveguides," *J. Communications Technology and Electronics* **44**,827(1999). Translated from *Radiotekhnika i Elektronika* **44**, 885(1999).

[19] For a discussion of various forms for chiral constitutive equations, see Ref. 2, chap. 3.

[20] C.F. Bohren, "Light scattering by an optically active sphere," *Chem. Phys. Lett.* **29**, 458(1974) and "Scattering of electromagnetic waves by an optically active spherical shell," *J. Chem. Phys.* **62**, 1566(1975). See also the discussion in Ref. 2, chap. 7 and Ref. 18.

[21] C.R. Paiva, A.L. Topa, and A.M. Barbosa, "Semileaky waves in dielectric chirowaveguides," *Optics Letters* **17**, 1670(1992).

[22] See for example, P.K. Cheo, Fiber Optics and Optoelectronics, 2nd Edition, (Prentice Hall, New Jersey, 1990), chapter 3.

[23] Solutions for all examples in this paper were obtained using built-in routines in Mathcad 2000 Professional (MathSoft, Inc., Cambridge, MA).

[24] The TE and TM mode equations are normally written using arctangent rather than arccotangent. However, the arguments of the arctangent are positive definite and arctan(x) = arccot($1/x$), for $x>0$ as is true for the achiral case. There is an advantage to using arccotangent in the chiral case because singularities of the argument cause π discontinuities of arccotangent only at the endpoints of the range $|g|<1$, while if arctangent is used, there are π discontinuities at $g = \pm r_0$ inside this range.

[25] For a discussion of semileaky waves in chiral waveguides, see Ref. 21.

[26] The modal dispersion equations in Ref.18 are written using normalized waveguide parameters. Here we have refrained from using normalized parameters because neither the normalization used in Ref.18 nor that used in Ref.12 can simultaneously be used to investigate both thickness and frequency dependence.